Design and Analysis of Micro-Solar Power Systems for Wireless Sensor Networks

Jaein Jeong, Xiaofan Jiang, David Culler
Computer Science Division, UC Berkeley
{jaein,fxjiang,culler}@eecs.berkeley.edu

***Abstract*— Wireless Sensor Networks are fundamentally limited by their energy storage resources and the power they obtain from their environment. Several micro-solar powered designs have been developed to address this important problem but little analysis is available on key design trade-offs. We develop a taxonomy of the micro-solar design space identifying key components, design choices, interactions, challenges, and trade-offs. Based on this taxonomy, we provide an empirical and mathematical analysis of two prominent designs of micro-solar power systems (Heliomote and Trio), and interpret the results to propose design guidelines for micro-solar power systems.**

***Keywords*— Micro-Solar Power Systems, Solar Energy Harvesting, Wireless Sensor Networks, Modeling, Empirical Analysis**

I. Introduction

Autonomous long-term monitoring of the environment is one of the wireless sensor network (WSN) visions. However, limitation of energy supply has constantly impeded the progress of WSNs towards large scales and true autonomous operations. In recent years, energy harvesting, especially solar energy harvesting, has become increasingly important as a way to improve lifetime and reduce maintenance cost of WSNs. Compared to well-studied macro-solar systems (e.g. electricity generation for residential and commercial buildings), solar energy harvesting for micro-solar systems is more constrained in energy budget and energy use, and is still under active research.

Several micro-solar powered designs have been developed from different institutions, each with a unique set of requirements, such as lifetime, simplicity, cost, etc [3], [5], [10]–[13], [15]. Heliomote [10] and Trio [3] represent two different points in this design space. Heliomote, in favor of simplicity, employs single-level energy storage and hardware-controlled battery charging, whereas, Trio is designed for lifetime and flexibility and employs two-level energy storage and software-controlled battery charging. They are evaluated according to their own sets of conditions, but provide little analysis on how well they perform in the entire range of situations encountered in micro-solar systems.

Our contributions in this paper are three-fold: first, we present a model for micro-solar systems and develop a taxonomy of the micro-solar design space identifying key components, design choices, interactions, challenges and trade-offs; second, we provide an empirical analysis of two well-studied designs as concrete examples of micro-solar powered systems; third, we propose a design guideline for micro-solar systems based on the analysis of previously designed systems.

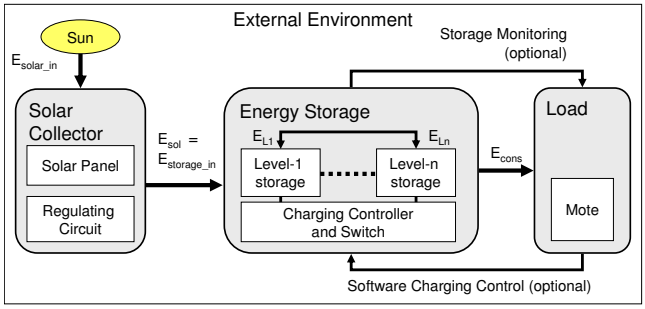

Fig. 1. Model for a solar-powered sensor system

The rest of this paper is organized as follows: section II presents a model for the micro-solar system; sections III, IV, V and VI show how each of the four components of a micro-solar power system models various design choices. Based on this model, section VII compares designs of Trio and Heliomote and analyzes the key design points that resulted in different characteristics and efficiencies. Section VIII concludes this paper.

II. System Architecture

In general, any solar-powered system consists of the following components: the external environment, the solar collector, energy storages, and the load (Figure 1). The solar energy from the environment is collected by the solar collector and is made available for the operation of the load. The energy storage is used to buffer the varying energy income and distribute it to the load over the entire duration.

The four components of a solar-powered sensor node interact with each other. The design decision for each component will dictate the energy flows between them and the overall behavior of the system. For the rest of this paper we will evaluate the performance of a micro-solar power system in terms of the energy flow of each component. Section III explains how to model the energy consumption of a mote (E_{cons}) with radio duty-cycling. Section IV shows how to estimate the solar radiation (E_{solar_in}) using statistical and mathematical methods. Section V discusses the factors that affect the solar-panel operating point (E_{sol}). Section VI discusses the factors that affects the storage capacity and the lifetime. Section VII shows how to measure the energy

TABLE I

EVALUATION METRICS

Metric	Description
E_{solar_in}	Total incident solar radiation.
E_{sol}	Energy produced by the solar panel.
$E_{storage\_in}$	Energy collected by the solar-collector.
$E_{L1}, \cdots, E_{Ln}$	Energy stored in level-i storage.
E_{cons}	Energy consumed by the mote.
r_{op-mpp}	Solar-collector matching metric: ratio of the deviation of solar-panel output power from the maximum output power.
Eff_{sys}	System-wide energy efficiency: energy for load consumption and net storage charge vs. incoming energy.
$\text{Eff}_{sol-out}$	Solar-collector efficiency: energy for load consumption and storage charging vs. energy from solar panel.
Eff_{Li-out}	Level-i storage efficiency: rate of level-i storage energy used for mote operation.

flow of the four components in a real experiment and evaluates the performance of Trio and Heliomote based on the measurement. Table I lists the metrics that will be used through this paper.

Our study is focused on the energy harvesting for micro-solar power systems such as solar-powered sensor nodes. Compared to well addressed macro-solar power systems (e.g. electricity generation for residential and commercial buildings), micro-solar power systems have the following characteristics: (1) energy budget is small due to size constraint; (2) energy consumption by controlling devices (e.g. charging controller, regulator) takes a large fraction of the energy budget; (3) there is substantial interaction among the solar-powered system components.

III. LOAD: SENSOR NODE

The sensor node (mote) is the end consumer of energy in a micro-solar power system. The amount of energy a mote consumes (E_{cons}) determines the capacity planning of a solar-powered sensor node. In order to size the mote energy consumption, we need to understand its main causes of energy consumption: radio communication and sensing. Since a mote draws much higher current when its radio-chip is awake, radio duty-cycling is commonly used as a technique to save the energy consumption of a mote. Power savings for the sensing device can be achieved in a similar way. A mote's current consumption rate I_{est} can be estimated with the formula below if the current consumption rates for the sleep state and the active state (I_{sleep} and I_{awake}) are known:

$$I_{est} \quad = \quad R \cdot I_{awake} + (1 - R) \cdot I_{sleep}$$

The experimental result that compares the current consumption measurements (I_{avg}) and the estimates for different radio duty-cycle rates (I_{est}) is shown in Table II. The small difference between the measurements and the estimates (-1.62% to 0.61%) implies that we can estimate the current consumption of a mote as a simple function of the duty-cycle rate R ($0 < R < 1$). Although we show radio duty-cycling for a single sensor node, the concept is still valid for a network of sensor nodes using low-duty cycle MAC (Media Access Control) protocols [8], [14]. In order to adjust the radio duty cycle according to energy availability, we can use the techniques in the literature [4]–[7].

TABLE II

CURRENT CONSUMPTION OF THE TRIO NODE AT SLEEP AND AWAKE STATES FOR DIFFERENT DUTY-CYCLE RATES.

	1.56%	**6.25%**	**12.5%**	**25%**	**50%**
I_{avg} (mA)	0.528	1.327	2.408	4.569	8.854
I_{sleep} (mA)	0.264	0.265	0.276	0.275	0.319
I_{awake} (mA)	17.414	17.342	17.355	17.306	17.362
I_{est} (mA)	0.536	1.338	2.405	4.541	8.812
$\frac{I_{avg}-I_{est}}{I_{est}}$	-1.62%	-0.79%	0.12%	0.61%	0.47%

IV. EXTERNAL ENVIRONMENT

The amount of solar radiation E_{solar_in} depends on the environment, and places an upper bound on the maximum energy output of the solar collector E_{sol}. Most previous designs of micro-solar power sensor systems did not carefully model the solar radiation: they either paid little attention to the available solar energy or considered a constant average solar radiation [3], [5], [10]–[13]. Kansal *et al.* [6] proposed a rule for perpetual operation, which stated a relationship between the node consumption and the energy budget. However, this rule considered a generic energy input and did not provide a way to estimate the energy budget for solar energy harvesting.

In this paper, we describe two ways to estimate the solar radiation: a statistical method and an astronomical method. With a statistical method, we estimate the solar radiation for a given period using the history of solar radiation. In order to get the statistics, we can use meteorological database software suite such as *Meteonorm* [1], which estimates the solar energy radiation as the monthly solar radiation E_{month} (kWh/m^2). Using E_{month}, we can calculate the peak solar hours (PSH), which is the equivalent solar radiation hours per day assuming that the same amount of solar energy is given at an intensity of $1kW/m^2$. Then, the available energy from a specific solar panel for one day, E_{sol}, can be estimated as the product of PSH and the solar panel output power P_{solar} at $1kW/m^2$ (usually provided by its manufacturer) :

$$E_{sol} = \text{PSH} \cdot P_{solar} = \frac{E_{month} \cdot P_{solar}}{1kW/m^2 \cdot \#\text{days}}$$

With an astronomical model, we estimate the solar radiation using the parameters that affect the angle between the sunlight and the solar panel. When the angle of sunlight from the normal to the solar panel is Θ, the effective sunlight that shines on the solar panel is proportional to $\cos\Theta$ [2]. The angle Θ depends on solar-panel inclination θ_p, panel orientation ϕ_p, latitude L, time of the day t, and day of the year n. We can estimate the solar radiation for a time period using $\cos\Theta$. The daily peak solar hours (PSH) can be given as follows:

$$PSH = \int_{t_{sunrise}}^{t_{sunset}} \cos\Theta dt$$

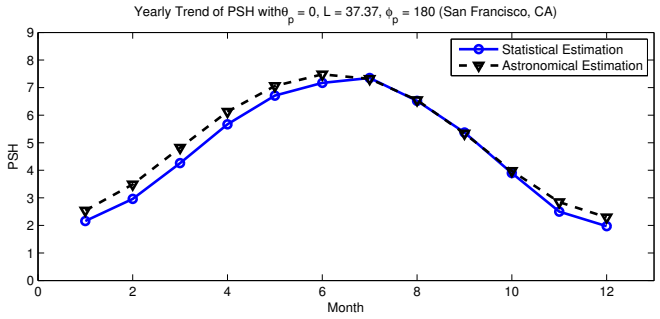

Fig. 2. Comparison of statistical and astronomical estimations of daily PSH for each month at San Francisco, CA with latitude 37.37°N

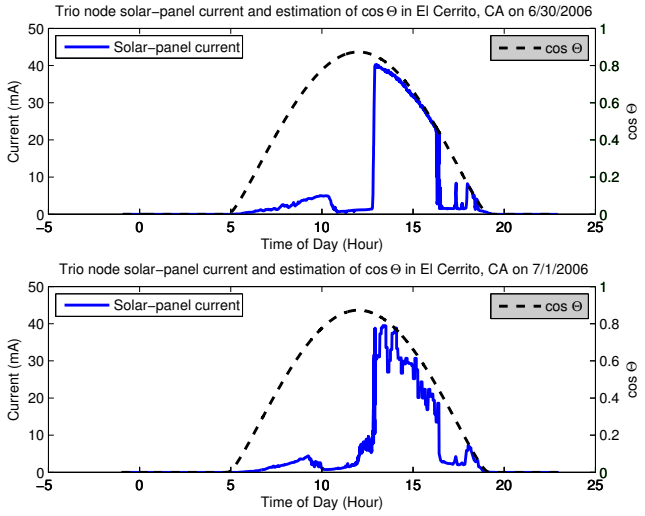

Fig. 3. Effects of obstruction and diffusion. The gap between the solar-panel current measurement and astronomical estimation shows the obstruction effect (5 AM to 1 PM and 4 PM to 5 PM). The gap during the radiation hours (1 PM to 4 PM) shows the diffusion effect.

Figure 2 compares the PSH estimation with statistical and astronomical models. In dry season, they closely match within 5%. Even in rainy season, the astronomical model differs within 15% from the statistical method.

The actual solar radiation may deviate from the statistical or astronomical estimate when it is obstructed by other objects or diffused by the clouds. We can estimate the effect of obstruction if we have a sample of solar radiation profile, and this is based on the fact that most obstructions are caused by stationary objects (e.g. buildings and trees) and the pattern is similar for each day (Figure 3). The difference between astronomical and statistical models in Figure 2 implies that there is more diffusion when the difference between the two is higher. We can model the diffusion effect probabilistically by making the diffusion probability proportional to this difference.

V. Solar Collector

Solar energy from the environment is converted to electric energy by the solar collector which includes a solar panel and a regulator. The solar panel converts photons into electricity

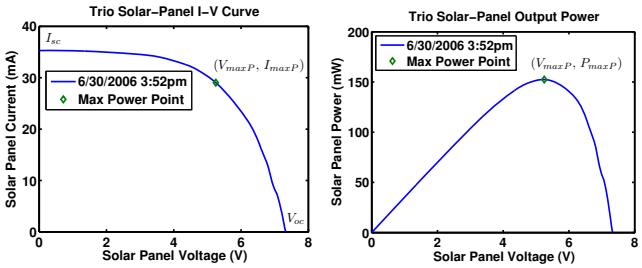

Fig. 4. Solar-panel: (a) I-V characteristic, (b) V-P graph with MPP

and the regulator conditions the output power of the solar panel for energy transfer to the storage. The amount of solar energy out of the solar collector E_{sol} is determined by the following factors: (1) solar radiation, (2) solar-panel characteristics, (3) the operating point of solar-panel. The solar-panel I-V (current-voltage) curve describes how the output current of a solar panel behaves at a certain radiation condition. (Figure 4). The solar panel outputs the maximum power when the product of current I and voltage V is maximum. As the solar irradiance increases or decreases, the I-V curve moves outwards or inwards. Thus, a solar panel can be described as a sequence of I-V curves with each I-V curve corresponding to a particular solar irradiance condition (Figure 7). The regulator protects the energy storage from being drained under low radiation, protects the energy storage from overload, and sets the operating point for the solar panel.

In order to maximize the power transfer from the solar panel, it is recommended that the regulating circuit operate near maximum power point (MPP), which is the point in the I-V curve where $P = I \cdot V$ is maximized. As a way of achieving maximum power transfer, a maximum power point tracker can be used (e.g. Everlast [13]). An active circuit is usually required when the energy signal is near DC (Direct Current). While this may sound like an attractive option, care needs to be taken when using it in practice. Since the power a sensor node operates at is usually very small (in the mW range), the energy consumed by the maximum power point tracker becomes significant and sometimes more than what it can save.

VI. Energy Storage

Energy storage is comprised of a group of elements used to buffer the energy coming from the solar collector and deliver them to the mote in a predictable fashion. Designing the energy storage involves choosing the storage elements and charging mechanism for correct operation and efficient energy transfer while satisfying a set of system requirements such as lifetime, capacity, current draw, size and weight. For the energy storage element, NiMH (Nickel Metal Hydride) or Li+/Li-polymer (Lithium-ion / Lithium polymer) batteries are desirable due to their high energy density; supercapacitors are desirable due to their high charge cycles.

A single energy storage element is traditionally used due to its simplicity, however, a combination of storage elements with different capabilities can often be used to improve

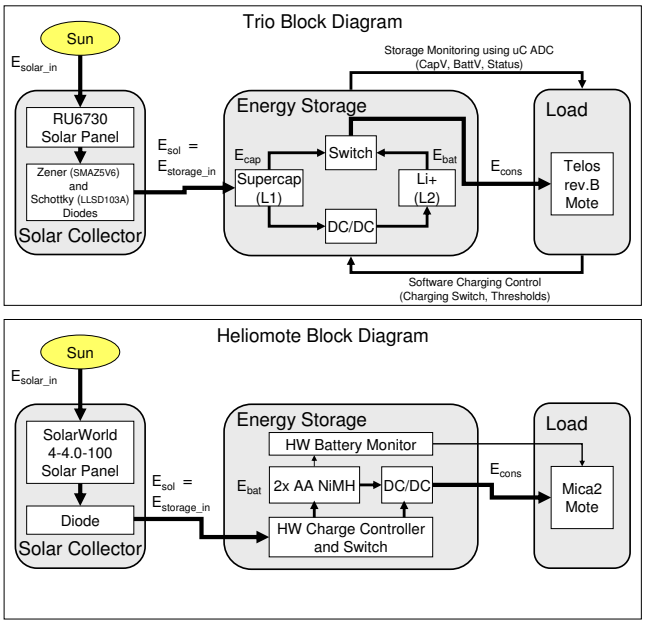

Fig. 5. Block diagrams for Trio and Heliomote

lifetime and capacity. Short frequent disruptions are buffered by smaller capacity storages while larger but less frequent disruptions are buffered by larger capacity storages. In this way, small disruptions do not affect the lifetime of larger storage element, which may often have less charge cycles. Different energy storages have different charging profiles, and require charging mechanisms of varying complexities. Depending on the system requirements, the correct point between the trade-off of complexity and energy transfer efficiency needs to be determined.

VII. Comparative Study

To provide a concrete understanding of micro-solar systems, we compare Trio [3] and Heliomote [10], as modeled in Figure 5. These two systems have been widely deployed and show different design points in this space. Trio uses two-level storage (supercapacitors and Li+ battery), software-controlled charging and regulation in favor of flexibility and efficiency. Heliomote, on the other hand, uses single-level storage (NiMH battery), hardware-controlled charging and regulation for simplicity. In this section, we compare the empirical data of the two systems and analyze how system performance is affected by different design decisions.

A. Solar-Collector Operation

1) Experimental Setup: We evaluate solar collector performance of each system by comparing the ratio of the deviation of the solar panel output power P_{op} from the maximum output power P_{maxP}:

$$r_{op-mpp} = |P_{op} - P_{maxP}|/P_{maxP}$$

where P_{op} is the solar-panel output power at the operating point and represents the actual power delivered to the next stage. P_{maxP} is the maximum possible output power

Algorithm 1 Trio battery charging algorithm

if ($V_{bat} < V_{bat-ub}$ and $V_{cap} < V_{cap-lb}$) **then**
  Stop charging.
else if ($V_{bat} < V_{bat-ub}$ and $V_{cap} \geq V_{cap-ub}$) **then**
  Start charging.
else if ($V_{bat} \geq V_{bat-ub}$) **then**
  Stop charging.
end if

that can be achieved with maximum power point tracking, and represents the theoretical maximum. We performed experiments to measure P_{op} and P_{maxP}. In experiment (a), we measured the solar-panel operating voltage (V_{op}) and current (I_{op}) to calculate $P_{op} = V_{op} \cdot I_{op}$. In experiment (b), we measured the characteristic of a separate solar panel by adjusting the load impedance in multiple steps to read a sequence of (I,V) pairs. Based on this set of I-V curves, we can find the maximum output power $P_{maxP} = V_{maxP} \cdot I_{maxP}$, where V_{maxP} and I_{maxP} are the voltage V and the current I in the I-V curve that maximize the product $V \cdot I$. This experiment was executed at Richmond Field Station in Richmond, California with a non-obstructed view of sunlight. Fluke-189 data logging multimeters were used to record measurements. In comparing the two systems, we focus on high radiation hours (9AM to 5PM) because solar panel output current is too small for practical use outside this time window.

2) Results: Figure 7 shows a series of I-V curves of solar panels from Trio and Heliomote nodes; each I-V curve is marked with corresponding operating point and maximum power point. The solar panel output power (P_{op}) and the maximum possible output power (P_{maxP}) for each I-V curves are shown in Table III and Figure 8. From the comparison result of P_{op} and P_{maxP}, we can see that the solar-collector of Trio is better matched to the maximum power point than that of Heliomote.

The average deviation of P_{op} from P_{maxP} is 4.83mW (5.3%) for Trio whereas it is 16.75mW (23.2%) for Heliomote. This gap is due to the design of the solar-panel regulator and the storage charging controller, as shown in Figure 10. For Trio, solar panel output is buffered in the supercapacitor before charging the battery. The supercapacitor operates between 3.2V and 4.0V. This range is set by thresholds V_{cap-lb} and V_{cap-ub} in the software-based charging controller (Algorithm 1). The overload protection voltage $V_{overload}$ is set to 5.1V by the reverse-biased Zener diode. Thus, the solar panel output can be transferred to the supercapacitor and the battery without being cut by the overload protection circuit. Heliomote, on the other hand, charges the solar-panel output to the battery without buffering and the solar-panel operating voltage V_{op} is clipped to the overload protection voltage $V_{overload}$ (= 2.8V). While this protects the battery from overload, more of the energy from the solar panel is wasted causing the larger deviation from P_{maxP}.

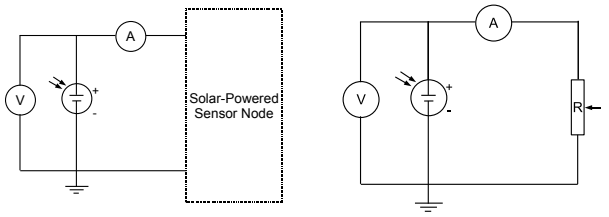

(a) (b)

Fig. 6. Experiment set-up for measuring solar panel output power.

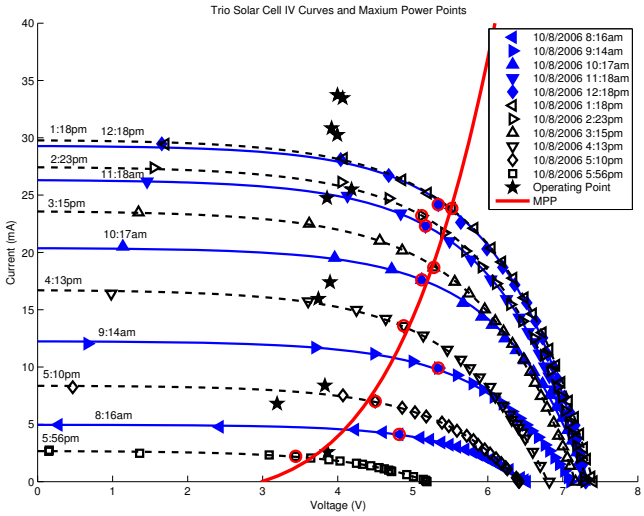

(a) Trio

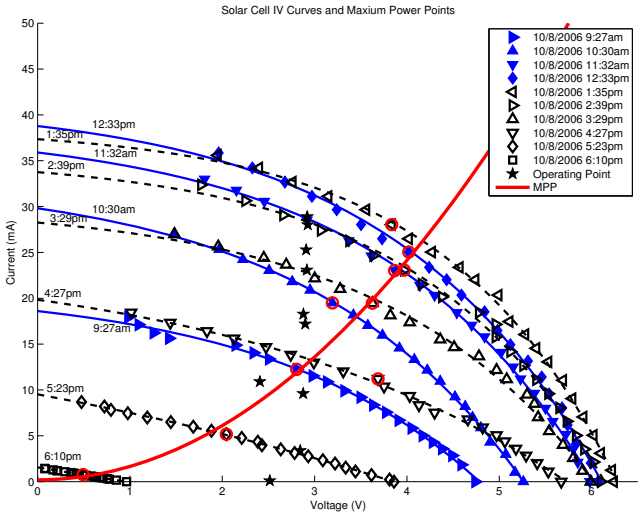

(b) Heliomote

Fig. 7. I-V characteristics of solar panels

TABLE III
MEASUREMENT OF SOLAR-PANEL CHARACTERISTICS FOR TRIO AND THE HELIOMOTE (10/8/2006).

Trio				
Time	I_{sc}(mA)	V_{oc}(V)	P_{maxP}(mW)	P_{op}(mW)
8:16 AM	4.96	6.52	19.90	21.72
9:14 AM	12.04	7.10	52.96	59.67
10:17 AM	20.51	7.28	90.37	95.50
11:18 AM	26.18	7.30	115.55	120.85
12:18 PM	29.47	7.31	129.07	134.83
1:18 PM	29.45	7.41	131.65	136.10
2:23 PM	27.38	7.29	118.88	120.81
3:15 PM	23.49	7.17	98.81	106.69
4:13 PM	16.40	6.82	66.32	67.82
5:10 PM	8.24	6.42	31.61	32.09
5:56 PM	2.75	5.19	7.59	9.97
Heliomote				
Time	I_{sc}(mA)	V_{oc}(V)	P_{maxP}(mW)	P_{op}(mW)
9:27 AM	17.93	4.74	34.42	26.26
10:30 AM	26.92	5.26	62.37	52.59
11:32 AM	32.99	5.98	89.02	73.54
12:33 PM	35.85	6.07	100.66	84.38
1:35 PM	35.59	6.24	107.50	81.97
2:39 PM	32.37	6.10	91.56	67.34
3:29 PM	27.01	5.99	70.60	49.81
4:27 PM	18.43	5.67	41.42	27.62
5:23 PM	8.68	3.86	10.58	9.65
6:10 PM	1.44	0.96	0.38	0.24

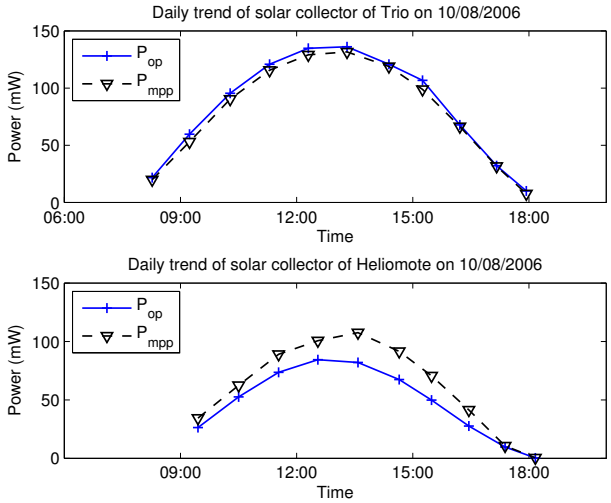

Fig. 8. Comparison of P_{op} and P_{maxP} for Trio and Heliomote

Figure 9 shows the relationship between solar panel output power P_{op} and the operating voltage V_{op} for the two system. P_{op} is close to zero for a large range of voltage levels, but rises sharply once the voltage is past a certain threshold (3.7V for Trio and 2.8V for Heliomote). This implies that the useful (most power produced) range of the solar panel in a particular system is very narrow. Therefore, power tracking circuits or algorithms are only meaningful within this small range.

B. Energy Flow and Energy Efficiency

1) Experimental Setup: As an evaluation metric of a micro-solar system, we propose the following efficiency

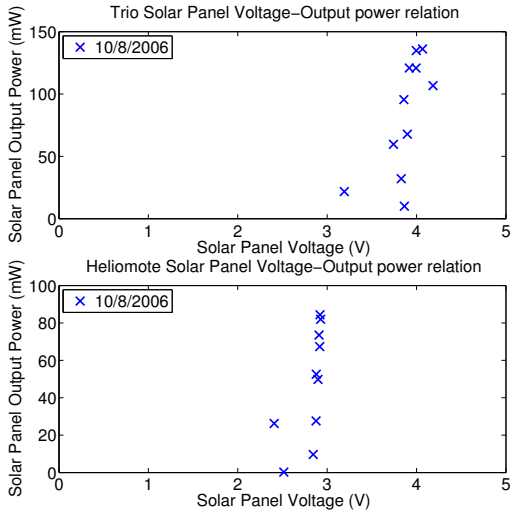

Fig. 9. Operating voltage to power relation for Trio and Heliomote.

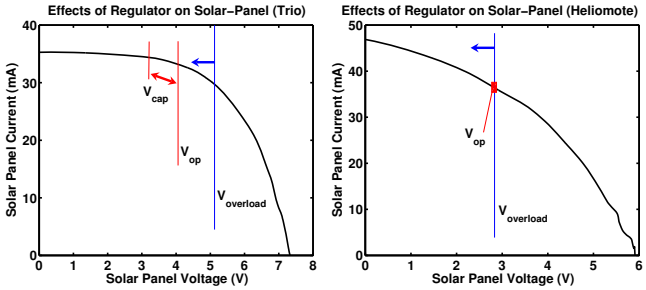

Fig. 10. Comparison of regulator design

metrics:

- System-wide efficiency: Eff_{sys}
- Battery discharging efficiency: $\text{Eff}_{bat-dis}$
- Capacitor discharging efficiency: $\text{Eff}_{cap-dis}$
- Charging efficiency: Eff_{chg}

These metrics are defined as follows:

$\text{Eff}_{sys} = (\Delta E_{bat} + \Delta E_{cap} + \Delta E_{cons})/\Delta E_{sol}$

$\text{Eff}_{bat-dis} = \Delta E_{cons}/\Delta E_{bat-dis}$

$\text{Eff}_{cap-dis} = \Delta E_{cons}/\Delta E_{cap-dis}$

$\text{Eff}_{chg} = (\Delta E_{bat-chg} + \Delta E_{cap-chg} + \Delta E_{cons})/\Delta E_{sol}$

Here, E_{bat} and E_{cap} are the balance of energy level for the battery and the supercapacitor for the given measurement time. Whereas $E_{bat-dis}$ and $E_{cap-dis}$ are the energy discharged from each storage, and $E_{bat-chg}$ and $E_{cap-chg}$ are the energy charged to each storage.

We set up the experiment as in Figure 11 and measured the following characteristics of Trio and Heliomote: solar panel voltage $V_{sol}(t)$, solar panel current $I_{sol}(t)$, and voltage levels of the energy storage elements ($V_{cap}(t)$ and $V_{bat}(t)$). Using this measurement data, we can calculate the energy budget and the stored energy for a given period. As for the mote operation, we use Telos rev. B [9] for both Trio and Heliomote. When we set the radio duty-cycle as 1.56%, the average current consumption for one-hour measurement I_{avg} is 0.5448mA (Trio) and 0.4031mA

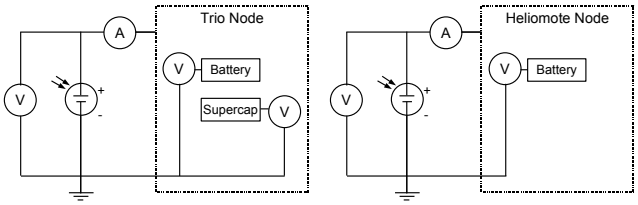

Fig. 11. Experiment setup for measuring energy efficiency (a) Trio, (b) Heliomote

(Heliomote). In order to calculate the energy stored in the battery E_{bat}, we estimate the voltage-to-energy relation using the manufacturer-provided voltage-to-capacity or voltage-to-discharge time profile.

2) Results: Table IV summarizes the trend of daily energy levels. First, it shows that the net battery energy level has increased, which means that Trio and Heliomote have excess energy to store even after mote consumptions and energy losses. Second, it shows that the supercapacitor of Trio stays at about the same energy level each day, with net increase close to zero. This implies that the supercapacitor buffers the solar energy, and transfers the excess energy to the battery. The net battery energy increase ΔE_{bat} is positively correlated with the daily solar energy budget ΔE_{sol}. Finally, our experiment data show that for the Trio node, 19.5% to 33.4% of the available solar energy is charged in the storage or consumed by the mote while the Heliomote node has the energy efficiency between 6.9% to 14.6%. As for the weather condition for the measurement on each day, we chose the sunny days in mid-October so that the weather condition is similar to all the measurements. One difference between the measurements of each day is the energy level of the storage elements. This is because we use the same experiment setup over multiple days without depleting the energy storage. This explains the difference in energy level of the storage elements (ΔE_{bat}).

In order to calculate the charging and discharging efficiencies, we can divide the operating range of Trio and Heliomote into multiple phases as shown in Figure 12 and Figure 13. In *battery discharge phase* (D1), the energy for load consumption is supplied by the energy discharged from the battery with no other incoming energy. In *capacitor discharge phase* (D2), the energy for load consumption is supplied by the energy discharged from the supercapacitor with no other incoming energy. In *charge phase* (C), the energy for load consumption is supplied by the solar energy, and the excess energy is stored in the storage. In *saturation phase* (S), the energy for load consumption is supplied by the solar energy, but the excess energy is wasted. The balance of energy level of each component for these phases are shown in Figure 14 and Figure 15.

The charging and discharging efficiency results are summarized in Table V. Trio node has both a battery discharge phase and a capacitor discharge phase because it has two-

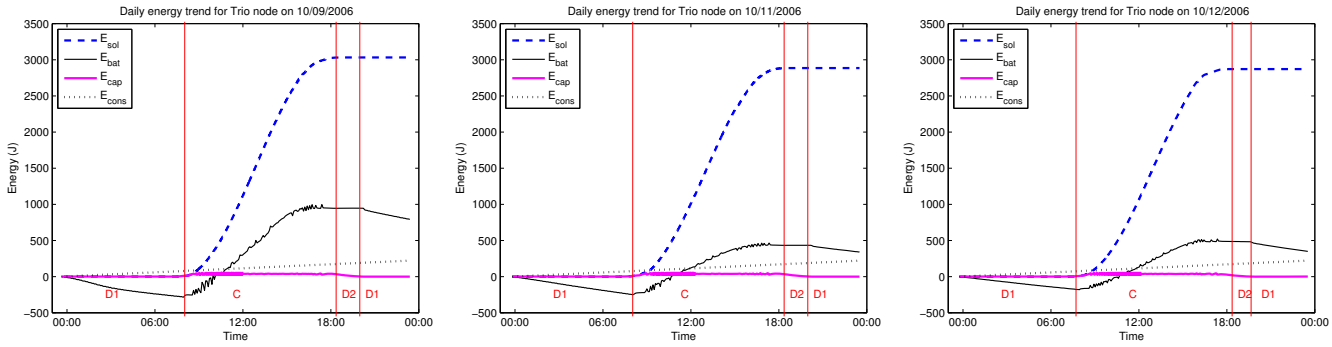

Fig. 12. Daily energy flow of Trio node. (a) 10/09/2006, (b) 10/11/2006, (c) 10/12/2006

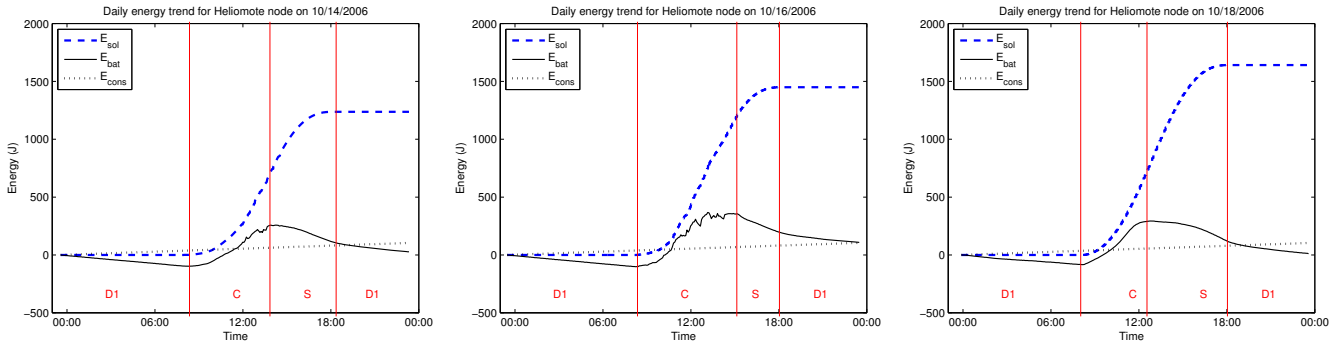

Fig. 13. Daily energy flow of Heliomote node. (a) 10/14/2006, (b) 10/16/2006, (c) 10/18/2006

level storage of supercapacitor and Li-ion battery. Trio also has a charge phase, but not a saturation phase. We observed the battery discharging efficiency of 24.5% to 34.9%, capacitor discharging efficiency of 54.3% to 68.6%, and charging efficiency of 28.5% to 46.9%. Heliomote node has battery discharge phase and a charge phase. It has a saturation phase and this is because the charging protection circuit is activated during its operation. We observed the battery discharging efficiency of 32.2% to 35.6% and charging efficiency of 45.5% to 54.2%.

We can see that the charging and discharging efficiency of Heliomote is as good as that of Trio but its system efficiency (6.9% to 14.6%) is much smaller than that of Trio (19.5% to 33.4%). This is because much of solar energy is wasted during the saturation phase. At a lower battery capacity, the system efficiency would be higher. If we assume that Heliomote does not go through the saturation phase and utilizes the solar energy during saturation phase as the same rate as in charging phase, then the system efficiency would be 31.9% to 41.9%.

Our experimental results also show that using two-level energy storage helps reduce the battery discharge frequency, thus saves the effective lifetime of the battery. From Figure 12, we can see that Trio uses the supercapacitor as its power source in charging phase (C) and capacitor discharging phase (D2). During this time, the supercapacitor cycles between charging and discharging, while the energy level of the Li^+ battery monotonically increases (except the spikes, which are the artifacts of short pulse charging). Whereas,

TABLE IV
ENERGY LEVEL OF EACH COMPONENT AND SYSTEM ENERGY EFFICIENCY FOR TRIO AND HELIOMOTE

Trio	Date	10/9/06	10/11/06	10/12/06
	ΔE_{sol}	3031.3J	2885.5J	2870.8J
	ΔE_{cap}	-0.05J	-0.04J	0.16J
	ΔE_{bat}	791.2J	342.1J	348.8J
	ΔE_{cons}	221.0J	220.3J	221.0J
	Eff_{sys}	33.4%	19.5%	19.8%
Heliomote	Date	10/14/06	10/16/06	10/18/06
	ΔE_{sol}	1237.6J	1449.9J	1641.4J
	ΔE_{bat}	27.0J	107.3J	10.1J
	ΔE_{cons}	10.0J	104.5J	103.0J
	Eff_{sys}	10.5%	14.6%	6.9%

Heliomote handles the charging-discharging cycle directly from the battery and the battery is discharged for longer hours (Figure 13).

VIII. CONCLUSION

To evaluate various design choices and provide guidelines for designing micro-solar systems, we have presented a system model and analyzed two published solar-powered sensor platforms, Trio and Heliomote. The analysis of our model and the observation of the two platforms give us some insight in how to design micro-solar systems.

For the solar-collector, we have observed that the range of solar-panel voltages that generate useful output power is narrow. Thus, we can closely match the solar-panel operating point to maximum power point by setting the operating

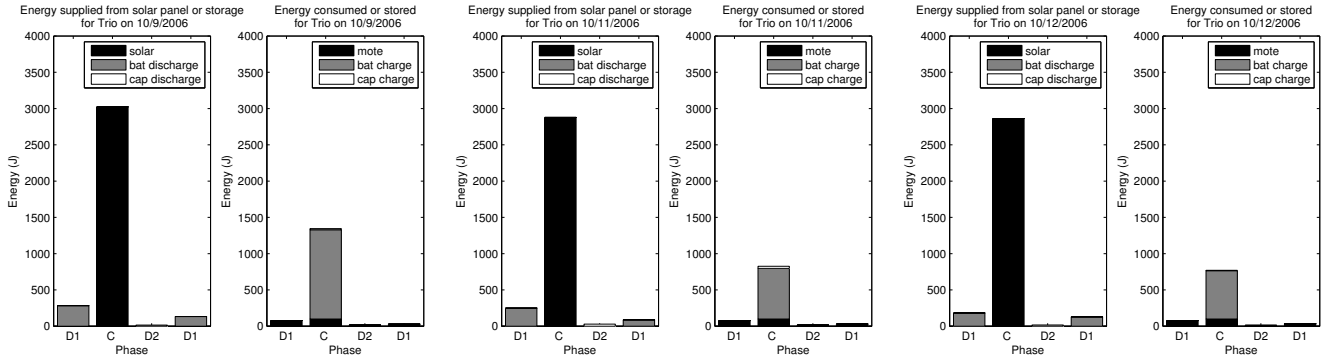

Fig. 14. Energy flow of Trio node at different phases. (a) 10/09/2006, (b) 10/11/2006, (c) 10/12/2006

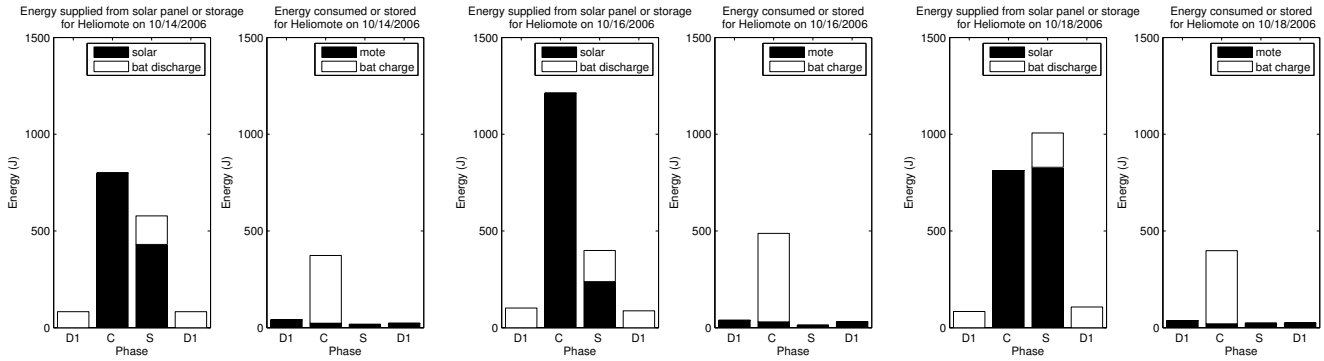

Fig. 15. Energy flow of Heliomote node at different phases. (a) 10/14/2006, (b) 10/16/2006, (c) 10/18/2006

TABLE V
ENERGY EFFICIENCY OF CHARGING AND DISCHARGING OPERATIONS FOR TRIO AND HELIOMOTE

Trio	Date	10/9/06	10/11/06	10/12/06
	Eff_{chg}	46.9%	31.2%	28.5%
	$\text{Eff}_{bat-dis}$	24.5%	32.7%	34.9%
	$\text{Eff}_{cap-dis}$	57.2%	54.3%	68.6%
Heliomote	Date	10/14/06	10/16/06	10/18/06
	Eff_{chg}	52.0%	45.5%	54.2%
	$\text{Eff}_{bat-dis}$	35.6%	32.2%	32.7%

point to this range without using a maximum power point tracking circuit. For energy storage, we have observed that using multi-level energy storage improves system-wide energy efficiency by buffering solar-collector output to a storage element with more desirable characteristic towards operating-point matching. We have also observed that using multi-level energy storage helps improve lifetime by reducing the number of charge-discharge cycles to cycle-sensitive storage elements.

The raw data and scripts for our experiments can be found at the web page `http://www.cs.berkeley.edu/~jaein/inss08_data/`.

REFERENCES

[1] Meteonorm. `http://www.meteotest.ch/pdf/am/mn_description.pdf`.

[2] J. V. Dave, P. Halpern, and H. J. Myers. Computation of Incident Solar Energy. *IBM Journal of Research and Development*, 19(6):539–549, 1975.

[3] P. Dutta, J. Hui, J. Jeong, S. Kim, C. Sharp, J. Taneja, G. Tolle, K. Whitehouse, and D. Culler. Trio: Enabling sustainable and scalable outdoor wireless sensor network deployments. *IEEE SPOTS*, 2006.

[4] J. Hsu, S. Zahedi, A. Kansal, and M. B. Srivastava. Adaptive duty cycling for energy harvesting systems. *IEEE ISLPED*, 2006.

[5] X. Jiang, J. Polastre, and D. Culler. Perpetual environmentally powered sensor networks. *IEEE SPOTS*, 2005.

[6] A. Kansal, D. Potter, and M. B. Srivastava. Performance aware tasking for environmentally powered sensor networks. *ACM SIGMETRICS*, 2004.

[7] C. Moser, D. Brunelli, L. Thiele, and L. Benini. Real-time scheduling with regenerative energy. *ECRTS*, 2006.

[8] J. Polastre, J. Hill, and D. Culler. Versatile low power media access for wireless sensor networks. *ACM Sensys*, 2004.

[9] J. Polastre, R. Szewczyk, and D. Culler. Telos: Enabling ultra-low power wireless research. *IEEE SPOTS*, 2005.

[10] V. Raghunathan, A. Kansal, J. Hsu, J. Friedman, and M. Srivastava. Design considerations for solar energy harvesting wireless embedded systems. *IEEE SPOTS*, 2005.

[11] S. Roundy, B. P. Otis, Y.-H. Chee, J. M. Rabaey, and P. Wright. A 1.9ghz rf transmit beacon using environmentally scavenged energy. *IEEE ISLPED*, 2003.

[12] P. Sikka, P. Corke, P. Valencia, C. Crossman, D. Swain, and G. Bishop-Hurley. Wireless adhoc sensor and actuator networks on the farm. *IEEE SPOTS*, 2006.

[13] F. Simjee and P. H. Chou. Everlast: Long-life, supercapacitor-operated wireless sensor node. *IEEE ISLPED*, 2006.

[14] W. Ye, J. Heidemann, and D. Estrin. An energy-efficient mac protocol for wireless sensor networks. *IEEE INFOCOM*, 2002.

[15] P. Zhang, C. M. Sadler, S. A. Lyon, and M. Martonosi. Hardware design experiences in zebranet. *ACM Sensys*, 2004.